Available online at www.sciencedirect.com

ScienceDirect

Procedia Structural Integrity 28 (2020) 1733–1744

Structural Integrity Procedia

www.elsevier.com/locate/procedia

1st Virtual European Conference on Fracture

Analysis of crack-tip constraint due to V- and U- side grooves in C(T) specimens

C. Soupramanien[a,*], S. Sivaprasad[a], Raghu V. Prakash[b]

[a]*Materials Mechanics Group, Materials Evaluation Division, CSIR-National Metallurgical Laboratory, Jamshedpur – 831007, India,*
[b]*Department of Mechanical Engineering, Indian Institute of Technology Madras, Chennai - 600 036, India*

Abstract

The effect of side grooves in standard compact tension (C(T)) specimens on the constraint due to plasticity under small scale yielding is presented in this paper. The Elastic-plastic crack-tip stress state is analysed through three dimensional finite element method. Ramberg-Osgood model is used to characterize the smooth transition of elastic-plastic behavior at the onset of crack-tip under Small Scale Yielding. Side grooves of type V and U are analysed and compared with plain specimen. Generally, it is observed that the plane stress effect on the surface of the plain specimen is restricted by the introduction of the side grooves. And this effect is studied with the in-plane crack-tip constraint parameter Q and out-of-plane constraint parameters T_z and h through the specimen thickness. It is found that localized plastic deformation at the side grooves increases the constraint level of the cracked specimen at the side grooves whereas it shows less at the middle of the specimen. It is also concluded that compared with U- groove specimen, V- groove specimen shows better constraint level.

*Keywords:*Crack-tip constraint; Fracture Toughness; Side groove effect

1. Introduction

Engineering critical assessment (ECA) methods such as BS 7910, API 579/ASME FFS-1 and R6 are developed for assessment of structural integrity of structures such as pressure vessels and pipelines that contain flaws or damage.

* Corresponding author. Tel.: +91-657-2345073; fax: +91-657-2345153.
E-mail address: csmanien@nmlindia.org

10.1016/j.prostr.2020.10.150

Nomenclature

B	Specimen Thickness
W	Specimen width
a	Crack length
a/W	normalised crack size
J	J-integral
J_{1C}	Plane-strain fracture toughness
CTOD	Crack-tip opening displacement
r, θ, z	polar co-ordinate at the crack-tip
σ_{xx}, σ_{yy}, σ_{zz}	Stress along different directions
σ_1, σ_2, σ_3	Principlal stress along different directions
α	yield offset in Ramberg-Osgood (RO) model
n	Strain hardening exponent in RO model
σ_0	yield stress
ε_0	yield strain

The calculated value of fracture parameters J-integral or Crack-tip opening displacement (CTOD) is compared with their critical value J_{IC} or $CTOD_{IC}$ to give the current state of damage and estimation of remaining life. International standards like ASTM E399-20 and E1820-20 are developed to quantify the fracture toughness of the materials in the testing laboratories and it is considered material property. It is also understood that the critical value J_{1C} or $CTOD_{1C}$ is not only material dependent but also depends on geometry of the specimens used in the laboratories (Anderson T.L., 2005; Kudari, S.K. et al.,2007). ASTM standards recommends specimen size requirements to validate the test result for both Linear Elastic Fracture Mechanics (LEFM) and Elastic-Plastic Fracture Mechanics (EPFM) conditions. Parameters such as specimen type, thickness, a/W ratio and load influences crack-tip condition which also affects the critical value J_{1C} or $CTOD_{1C}$. As a consequence, low fracture resistance is observed in a high crack-tip constrained specimen and high fracture resistance is observed in a low crack-tip constrained specimen (Matteo Chiesa et al., 2001)

In elastic-plastic fracture of specimen, large scale plastic deformations in plane stress mode occur near free surface (Imai Yasufumi et al., 1982; 1984). ASTM standards recommend the provision of side grooves in the test specimens to guide the crack to grow parallel to the crack line. The standard also recommends that the concentration of plasticity in the side grooves affects the crack-tip constraint more compared to the plain specimens. Absence of side grooves, the crack front may experience mixed mode fracture ahead of the crack-tip. Stress concentration factor (k_t) is higher in rectangular bar with opposite edge U-notches as compared to rectangular bar with opposite edge V-notches (Pilkey, Water D, 1997). Generally, researchers prefer V- side grooves over U- side grooves in the fracture toughness evaluation at the testing laboratory. But the change of side groove angle at the on-set of crack-tip is to be studied within the purview of the small strain theory. Two-dimensional analyses of specimens are not sufficient for precise understanding of the crack-tip conditions in side-groove specimens. Hence, in this paper 3-D elastic-plastic FEM work on C(T) specimens is carried out and the results analysed.

2. Constraint parameters

The ‘constraint effects in fracture’ is well established field of research in which geometrical effects are expressed in different constraint parameters and compared (ASTM STP1171, 1968; ASTM STP1244, 1995). In-plane constraint effects are studied with the two dimensional (2D) FEM study whereas out-of plane constraint effects are studied with three dimensional (3D) FEM analysis.

2.1. In-plane constraint parameters

Specimen geometry types, crack orientation, a/W ratio falls under In-plane study. T stress and Q stress constraint parameters are well known and used in LEFM and EPFM conditions respectively. In this paper, Q-stress is used to study the in-plane constraint effect. The stress field at the crack-tip in power-law hardening material with plasticity was introduced by HRR (Hutchinson, J.W., 1968; Rice, J.R., Rosengren, G. F., 1968). Later, taking reference from Williams, M., 1957, Sharma et al., 1991 introduced Q stress as second term in the HRR stress equation. Then, O'Dowd,

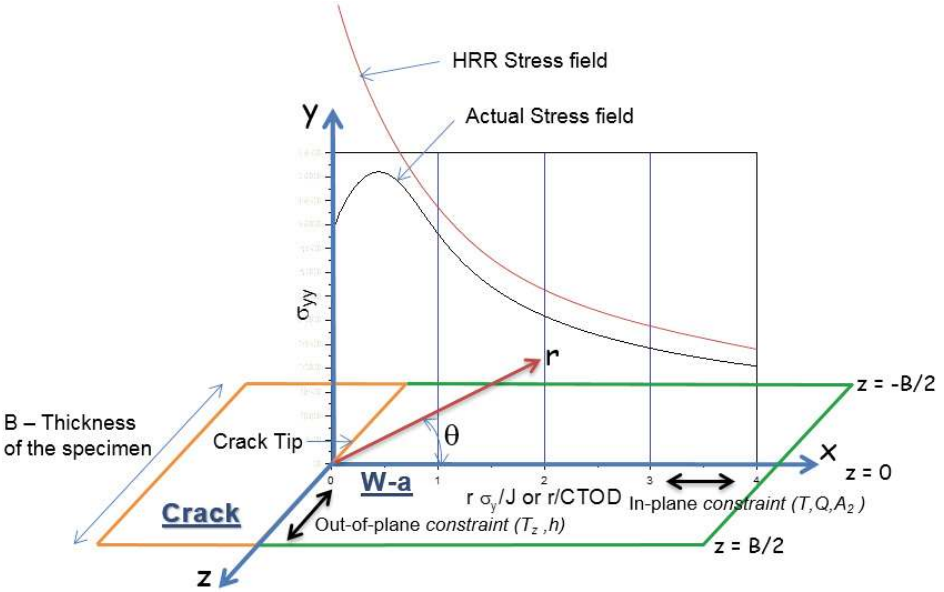

Fig. 1. Schematic illustration of in-plane and out-of-plane constraint conditions

N.P., et al. (1991) defined Q-stress using small scale yielding (SSY) distribution as shown in the equation 1.

$$Q = \frac{(\sigma_{\theta\theta})_{FEM} - (\sigma_{\theta\theta})_{SSY;T=0}}{\sigma_0}, for\ \theta = 0, \frac{r\sigma_0}{J} = 2 \quad (1)$$

Based on Robert H. Dodds et al., the equation 2 is used when the CTOD is applied.

$$Q = \frac{(\sigma_{\theta\theta})_{FEM} - (\sigma_{\theta\theta})_{SSY;T=0}}{\sigma_0}, for\ \theta = 0, \frac{r}{CTOD} = 4 \quad (2)$$

As CTOD is used as crack driving force, equation 2 is used in this analysis.

2.2. Out-of-plane constraint parameters

Three dimensional geometry effects, particularly test specimen thickness (TST) effect are studied using T_z and h constraint parameters. Guo Wanlin, 1993 introduced T_z as the triaxial stress constraint parameter which uses axial stresses at the crack-tip as shown in equation 3.

$$T_z = \frac{\sigma_{33}}{\sigma_{11} + \sigma_{22}} \quad (3)$$

The widely used parameter h (Henry, B.S. et al., 1997) takes principal stresses acting at the vicinity of the crack-tip to characterise the crack-tip constraint triaxially. In this study, both T_z and h were reported.

$$h = \frac{\sigma_m}{\sigma_{mises}} = \frac{\frac{\sigma_1 + \sigma_2 + \sigma_3}{3}}{\frac{\sqrt{(\sigma_1 - \sigma_2)^2 + (\sigma_2 - \sigma_3)^2 + (\sigma_3 - \sigma_1)^2}}{\sqrt{2}}} \quad (4)$$

3. Material Model

The SA333, Grade 6 is the material of this study, which is a carbon manganese steel sourced from the piping components used for primary heat transport in nuclear power plants. Cylindrical tensile specimens were fabricated from the pipe, with their loading axes parallel to the pipe axis. Extracting tensile parameters from the experimental tensile plot, Ramberg-osgood (RO) plasticity model (Eq (1)) with yield offset, $\alpha = 0.162$ and hardening exponent, $n = 7.47$ was used as material model in ABAQUS. Yield stress, σ_0 was determined from the tensile tests. The values of young's modulus and poisson's ratio were taken as 210 GPa and 0.3 respectively. In this analysis, the non-linear geometry option in ABAQUS was used. With axi-symmetric tensile simulation, RO model parameters are validated

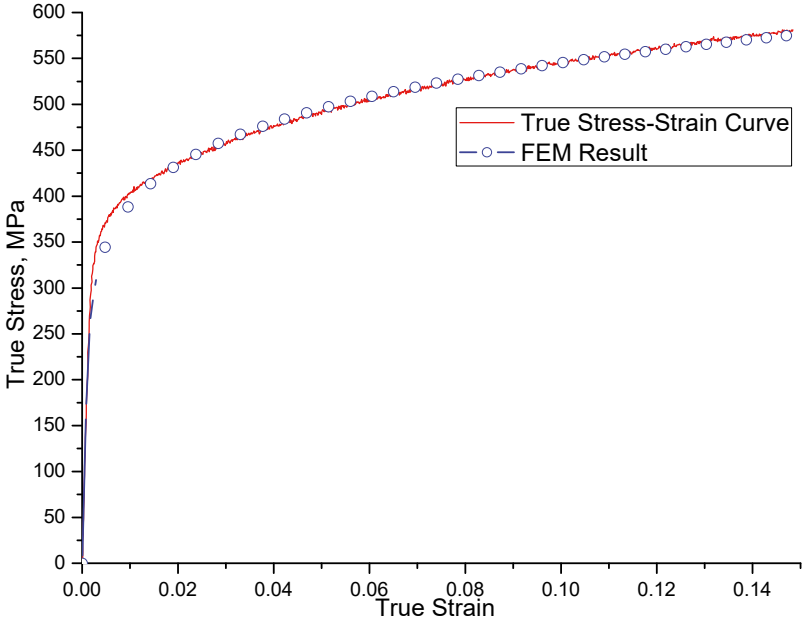

Fig. 2. Correlation of True stress-strain curve from experimental and FEM results.

in comparison with experimented true stress - true strain tensile results which is shown in fig. 2.

$$\frac{\epsilon}{\varepsilon_o} = \frac{\sigma}{\sigma_o} + \alpha \left(\frac{\sigma}{\sigma_o}\right)^n \tag{5}$$

4. FEM Methodology

4.1. 2D FEM

ABAQUS 2018 commercial software was used for the 2D and 3D finite element analyses. For Plane strain and Plane stress 2D Finite element analysis, full C(T) specimen geometry with W = 50 mm was used. Eight node plane strain element with reduced integration (CPE8R) in 2D Plane Strain (PE) FEA, eight node plane stress (PS) element with reduced integration (CPS8R) in 2D Plane Stress (PS) FEA as shown in Fig. 4(a) are used. Model is properly partitioned and structured mesh is applied around the crack-tip region. Modified Boundary Layer model as shown in fig. 3 along with axial displacement derived from Williams, M., 1957 are used to find the $\sigma_{\theta\theta}$ under Small Scale Yielding with T-stress = 0.

4.2. 3D FEM

As shown in fig. 5, Geometrical model of C(T) specimens with W=50 mm, B = 20 mm with the following side groove conditions are considered for 3D finite element analysis.

- Without side groove
- With U- side groove (angle = 0°)
- With V- side groove (angle = 45°)

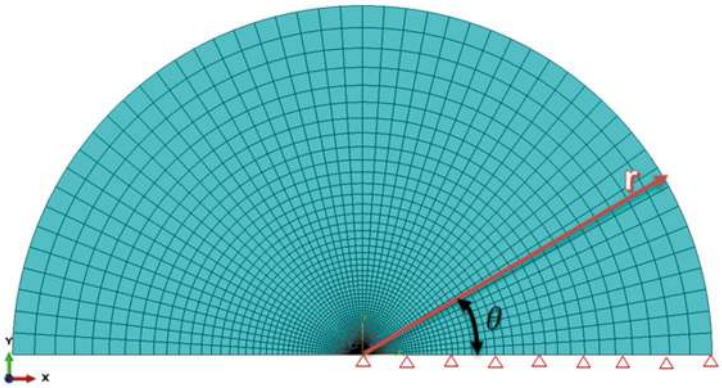

Fig. 3. Modified Boundary Layer model

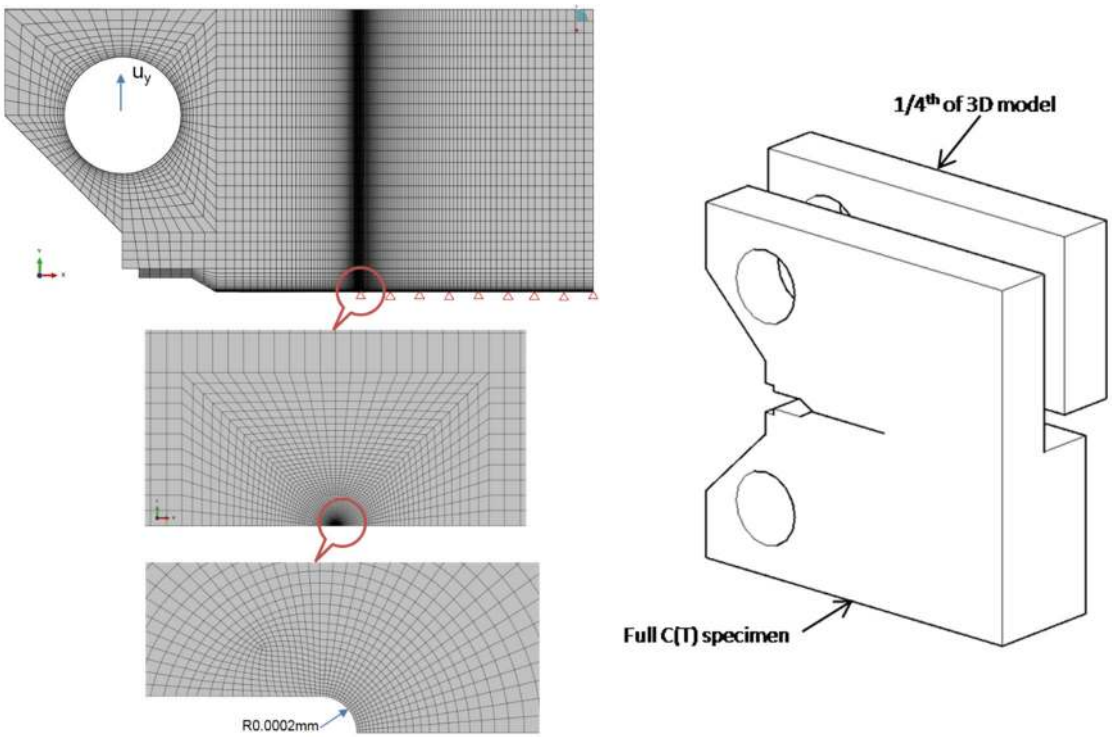

Fig. 4. Geometrical model of C(T) specimen (a) 2D with structured mesh at the crack-tip radius; (b) 3D model

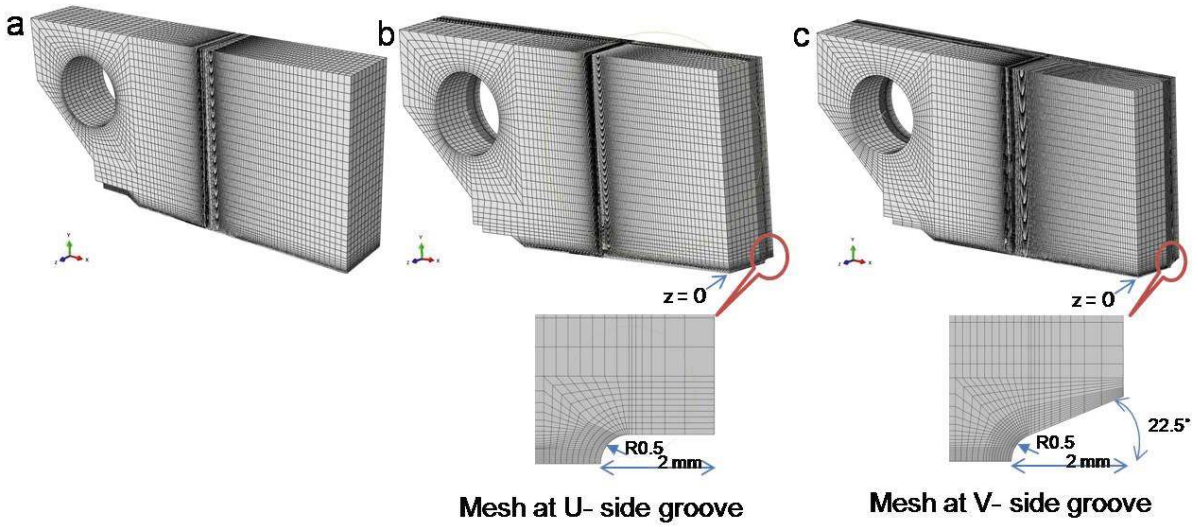

Fig. 5. 3D meshed C(T) specimen model (a) Plain (no groove) specimen; (b) U- side groove; (c) V- side groove

Depth of the side groove on both side of the specimens was 10% of the specimen thickness. For all conditions, a/W = 0.5 was modelled. 0.2μm of crack-tip radius was used in the 2D as well as 3D models. As shown in fig. 4(b), ¼ of the specimen geometry is used for FEA analysis to reduce no of elements and lower the computational time. Finite displacement with small increments is applied through a pin contact along the y direction. Symmetrical boundary conditions are provided at y and z directions. Z= 0 is denoted as middle of the specimen thickness and the front and back surface of the specimen are denoted as Z= B/2 & Z= -B/2 respectively. Eight noded three dimensional element with reduced integration (C3D8R) is used in 3D FEA. The thickness of the specimen and the notch radius are properly partitioned and meshed as shown in fig. 5. Focused mesh is arranged around the side groove radius which is similar to the mesh arrangement around crack-tip radius to provide better resolution in the results.

5. Results and Discussion

5.1. Crack-tip stress field

Stress field analysis at the threshold of the crack-tip was carried out on all 2D (SSY, PE, PS) and 3D (CT with Plain sided (no groove), V- and U- side groove) models. From the ABAQUS FEM analysis, stress components were extracted. Restricting PEEQ within r/CTOD = 1 in all results, the normalized opening mode stress with respect to r/CTOD is shown in fig. 6. It is observed that the opening mode stress in 3-D models are contained within the PE and PS stress conditions. Among the 3-D models, plain sided C(T) specimen shows higher stress than side grooved specimens. Also it is observed that stress level at V- grooved specimen is higher than the U- side grooved specimen. This shows that the introduction of side groove in the test specimen decreases the opening mode stress at the crack-tip. V- side grooved specimen shows better opening mode stress as compared with U-side grooved specimen.

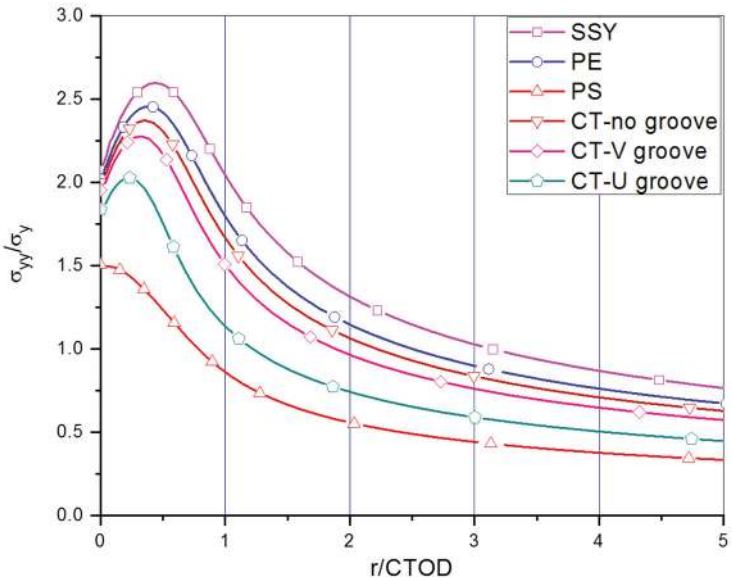

Fig. 6. Opening-mode stress distribution near the crack-tip along the ligament

The normalised crack opening mode stress with respect to half the specimen thickness is shown in fig. 7. For plain specimen, results are shown from middle of the specimen thickness to the surface, but for side grooved specimens, only up to 8 mm from the middle of the specimen thickness is shown. It is evident that due to the absence of side groove, high stresses are observed in the plain specimen at the middle of the thickness and slightly lower on the surface. In side grooved specimens, it is observed that stress at middle of the thickness is much lower than the free surface. This is due to concentration of plasticity that created the localized plane stress condition at the vicinity of the

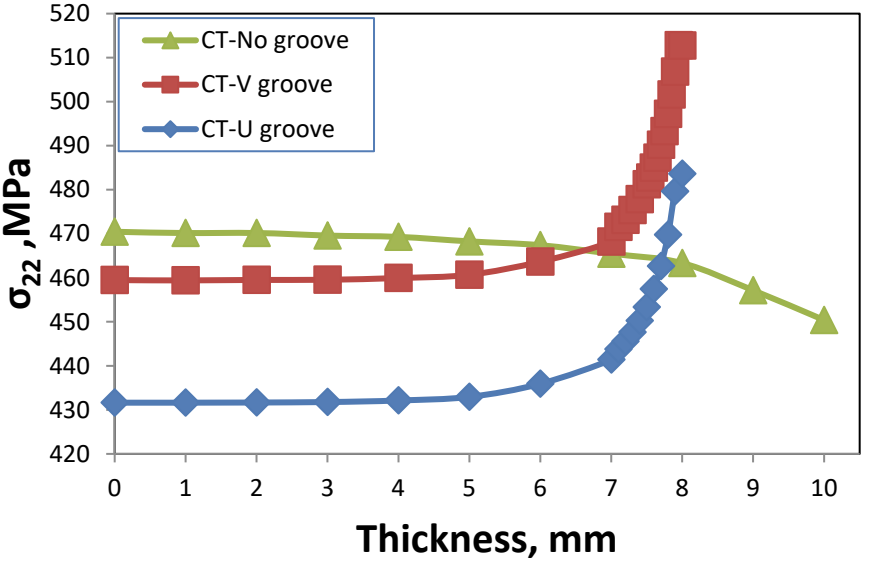

Fig. 7. Opening-mode stress distribution at the crack-tip across the specimen thickness

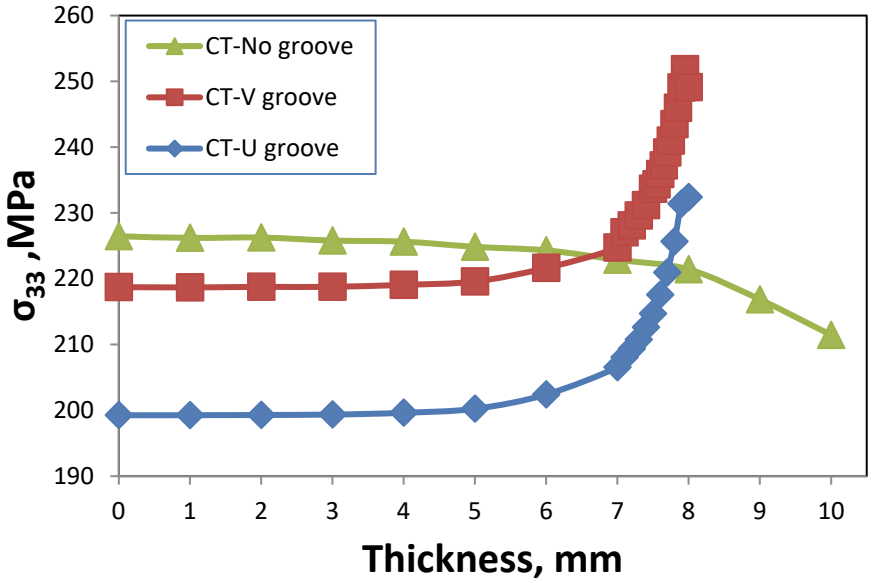

Fig. 8. S33 distribution at the crack-tip across the specimen thickness

side-groove. Among the types of side-grooved specimens used in this analysis, U- side grooved specimen shows lesser stress level along the thickness as compared to V-side grooved specimen.

Stress acting on thickness direction is shown in fig. 8. It follows the similar trend of opening mode stress distribution along the thickness of plain and side-grooved specimens. Under small strain analysis, it is observed that

the V- side grooves shows dominant over U- side grooves but slightly lower than the plain specimen. Due to concentration of plastic deformation at the side groove, material with high plasticity more freely deforms at the side groove than the middle of the specimen

5.2. *Effect on Crack driving force (CTOD)*

In this analysis, Crack-tip opening displacement (CTOD) is taken as crack driving force to explain the side groove effect at the on-set of the crack-tip. Fig. 9 shows the CTOD values obtained as per small stain theory from all the three 3D specimens which are normalised with CTOD value from the 2D Plane Strain analysis. Plain specimen records high CTOD at the middle of the specimen and slightly lower at the free surface of the specimen i.e., more crack front

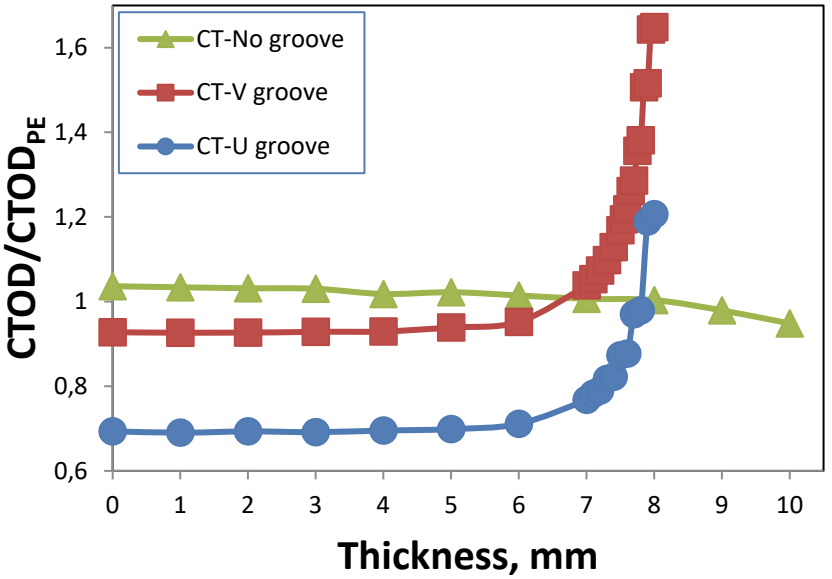

Fig. 9. Variation of CTOD at the crack-front across the specimen thickness

opening takes place at the middle of the thickness. It is observed that crack driving force in plain specimen is maintained on about 60% of the specimen thickness and then it gradually reduces towards the surface. But, side groove specimen records lower crack driving force at the middle and much higher at the side groove side as compared to plain specimen. It is evident that the tri-axial stresses acting at the side groove locally, weaken the crack driving force at the middle of the thickness. It is also understood that the CTOD measured by the Crack Opening Displacement (COD) gauge measures the lesser crack driving force experiencing at the middle of the thickness.

5.3. *Effect on Crack driving force (CTOD)*

Based on the crack-tip stress field data under small strain analysis, constraint effect of specimens with side grooves are analysed and presented in terms of constraint parameters Q (in-plane effect), T_z (Out of plane effect) and h (combined effect of in-plane and out of plane). Calculation of in-plane constraint parameter Q depends on crack opening mode stress, σ_{yy} and its effect along the thickness is shown in fig. 10. At middle of the specimen, the constraint level of the plain specimen is high as compared to side grooved specimens. It shows slightly loss of constraint at the surface and maintains uniform constraint on about 60 percent of the thickness. In side grooved specimens, V- grooved specimen shows better constraint level than U- groove specimen and it is closer to plain specimen. Both side grooved specimens shows higher constraint level at the side groove due to high crack opening stress observed locally.

Constraint parameter T_z expresses the thickness effect which is also called out-of-plane constraint. It is influenced by σ_{zz} which is normalised by the summation of σ_{xx} and σ_{yy}. In fig. 12 it is evident that the plain specimen maintains its high constraint level at the middle of the thickness and then reduces at the surface side. In side grooved specimens, V- grooved specimen shows more constraint level than U- grooved specimen but little less than the plain specimen. It is observed that the tri-axial stresses which acts locally at the side groove due to concentrated plastic deformation activity affects the constraint level not only at the middle of the thickness and also at the surface side. Taking in-plane and out-of-plane effects, the stress tri-axiality ratio $\frac{\sigma_h}{\sigma_e}$ is expressed in the constraint parameter 'h' which is shown in fig. 12. Provision of side groove reduces the constraint level at the middle of the specimen thickness but rises the constraint level at the side groove. Plain specimen shows highest level of constraint at the middle of the specimen among all specimens but drops a bit at the free surface. Also, it is observed that U- groove specimen shows poor constraint level than V- groove specimen and the difference of constraint level between plain specimen and V-groove

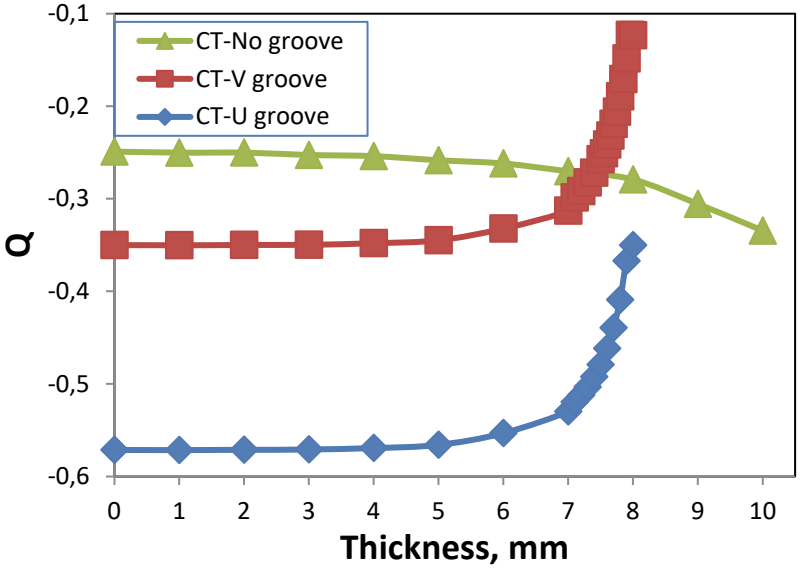

Fig. 10. Variation of the constraint parameter Q at the crack-tip across the specimen thickness

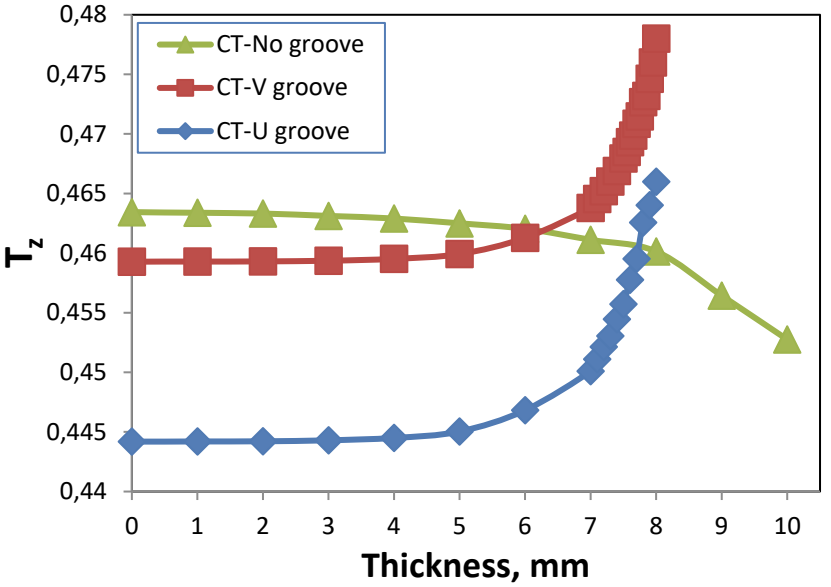

Fig. 11. Variation of the constraint parameter Tz at the crack-tip across the specimen thickness

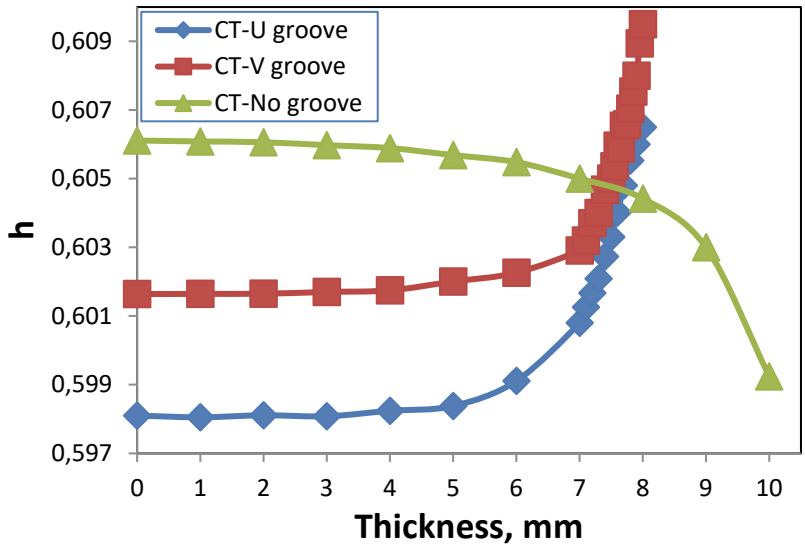

Fig. 12. Variation of the constraint parameter h at the crack-tip across the specimen thickness

specimen is wide. This may be due to the combined effect of in-plane and out-of-plane effect and it is clearly visible in the fig. 12. This is also evident that constraint parameter h captures the combined effect better than Q and T_z.

6. Conclusion

Three dimensional elastic-plastic finite element analysis of plain, U- and V- side grooved C(T) fracture specimen geometries are studied on the effect of crack-tip stress field, crack driving force and different constraint parameters across the thickness and the following conclusions are made.

- In side groove specimens, the crack driving force is experiencing more at the surface of the specimens due to high tri-axial stresses observed. In plain specimen, crack opening takes place more at the middle of the specimen thickness.
- Concentration of high local plastic deformation at the side groove weakens the constraint level of the side grooved specimens at the mid-thickness of the specimen but shows more at the side groove.
- Difference in constraint loss is captured better in constraint parameter 'h' analysis as compared to 'Q' and 'T_z'.
- In side grooved specimens, uniform constraint is observed on about 50 percent of the thickness.
- In comparison, U-groove specimen is found less constrained than V-groove specimen.

References

Abaqus® software documentation 2018

American Petroleum Institute/American Society of Mechanical Engineers, API 579/ASME FFS-1, Recommended practice for fitness-for-service, API, 2016.

Anderson T.L., Fracture mechanics: fundamentals and applications. 3rd ed. CRC Press; 2005.

ASTM E1820-20, Standard Test Method for Measurement of Fracture Toughness, ASTM International, West Conshohocken, PA, 2020

ASTM E399-20, Standard Test Method for Linear-Elastic Plane-Strain Fracture Toughness of Metallic Materials, ASTM International, West Conshohocken, PA, 2020

B.S. Henry, A.R. Luxmoore, The stress triaxiality constraint and the Q-value as a ductile fracture parameter, Engineering Fracture Mechanics, Volume 57, Issue 4, 1997, Pages 375-390

BS 7910:2005. Guide to methods for assessing the acceptability of flaws in metallic structures. British Standard Institution, London, UK, 2005.

Dodds, R.H., Anderson, T.L. & Kirk, M.T. A framework to correlate a/W ratio effects on elastic-plastic fracture toughness (J c). Int J Fracture, 48,

1991, 1–22
E. Hackett, K. Schwalbe, and R. Dodds, eds.,, STP1171-EB Constraint Effects in Fracture. West Conshohocken, PA: ASTM International, 1993
Hutchinson, J. W., Journal of Mechanics and Physics of Solids, Vol. 16, 1968, pp. 13-31.
Imai Yasufumi, Matake Tomokazu, Effect of side grooves on the elastic-plastic stress state of fracture toughness specimens—three-dimensional finite element analysis, Engineering Fracture Mechanics, Volume 16, Issue 5, 1982, Pages 659-668
Imai Yasufumi, Matake Tomokazu, Effect of Side Grooves for Three-point Bending Fracture Toughness Specimens : Three-dimensional Elastic-plastic Finite Element Analysis, Bulletin of JSME, 1984, Volume 27, Issue 227, p. 909-916
Kudari, S. K., Maiti, B., and Ray, K. K. The effect of specimen geometry on plastic zone size: a study using the J integral, J. Strain Analysis, 2007, 42, 125-136
M. Kirk and A. Bakker, eds.,, STP1244-EB Constraint Effects in Fracture Theory and Applicatons: Second Volume. West Conshohocken, PA: ASTM International, 1995
M. L. Williams, On the Stress at the Base of a Stationary Crack, Journal of Applied Mechanics, Transactions ASME, Vol. 24, 1957, pp. 109-114.
Matteo Chiesa, Bård Nyhus, Bjørn Skallerud, Christian Thaulow, Efficient fracture assessment of pipelines. A constraint-corrected SENT specimen approach, Engineering Fracture Mechanics, Volume 68, Issue 5, 2001, Pages 527-547
O'Dowd, NP, Shih CF (1991): Family of crack-tip fields characterised by a triaxial parameter-I. Journal of Mechanics and Physics of solids, Vol 39, pp.989-1015
Pilkey, Water D. Peterson's Stress Concentration Factors. Second Edition. New York:John Wiley & Sons, Inc., 1997.
R6, Revision 4, Assessment of the integrity of structures containing defects. EDF Energy, Gloucester, UK, 2015.
Rice, J. R. and Rosengren, G. F., Journal of Mechanics and Physics of Solids, Vol. 16, 1968, pp. 1- 12.
Rice, J. R., Journal of Applied Mechanics, Vol. 35, 1968, pp. 379-386.
Sharma, S. M. and Aravas, N., Journal of Mechanics and Physics of Solids, Vol. 39, 1991, pp. 1043- 1072
Toshiyuki Meshii, Kai Lu, Ryota Takamura, A failure criterion to explain the test specimen thickness effect on fracture toughness in the transition temperature region, Engineering Fracture Mechanics, Volume 104, 2013, Pages 184-197
Wanlin Guo, Elastoplastic three dimensional crack border field—I. Singular structure of the field, Engineering Fracture Mechanics, Volume 46, Issue 1, 1993, Pages 93-104